GEOPHYSICS, VOL. 64, NO. 6 (NOVEMBER–DECEMBER 1999); P. 1877–1889, 15 FIGS., 2 TABLES.

Source processes of industrially-induced earthquakes at The Geysers geothermal area, California

Alwyn Ross*, G. R. Foulger‡, and Bruce R. Julian**

ABSTRACT

Microearthquake activity at The Geysers geothermal area, California, mirrors the steam production rate, suggesting that the earthquakes are industrially induced. A 15-station network of digital, three-component seismic stations was operated for one month in 1991, and 3,900 earthquakes were recorded. Highly-accurate moment tensors were derived for 30 of the best recorded earthquakes by tracing rays through tomographically derived 3-D V_P and V_P/V_S structures, and inverting P- and S-wave polarities and amplitude ratios. The orientations of the P- and T-axes are very scattered, suggesting that there is no strong, systematic deviatoric stress field in the reservoir, which could explain why the earthquakes are not large. Most of the events had significant non-double-couple (non-DC) components in their source mechanisms with volumetric components up to ~30% of the total moment. Explosive and implosive sources were observed in approximately equal numbers, and must be caused by cavity creation (or expansion) and collapse. It is likely that there is a causal relationship between these processes and fluid reinjection and steam withdrawal. Compensated linear vector dipole (CLVD) components were up to 100% of the deviatoric component. Combinations of opening cracks and shear faults cannot explain all the observations, and rapid fluid flow may also be involved. The pattern of non-DC failure at The Geysers contrasts with that of the Hengill-Grensdalur area in Iceland, a largely unexploited water-dominated field in an extensional stress regime. These differences are poorly understood but may be linked to the contrasting regional stress regimes and the industrial exploitation at The Geysers.

INTRODUCTION

The Geysers is a steam-dominated geothermal reservoir that lies in the strike-slip stress regime of the San Andreas fault system in California (Figure 1). It has been heavily exploited for steam for electricity generation in recent years and production peaked in 1987 at about 3.5×10^3 kg s^{-1} of steam when 1800 MW of electricity were generated. Power production decreased subsequently in response to reservoir-wide steam pressure decline. Condensate is reinjected back into the reservoir in an attempt to mitigate this pressure decline. Since the reservoir pressure is less than hydrostatic, water is simply poured back into boreholes and sinks under gravity.

Steam extraction and fluid reinjection induce myriads of small earthquakes in the reservoir. The seismic rate is currently about 140 earthquakes larger than magnitude 1.2 per month. These earthquakes provide a rich source of information about the reservoir. Earthquake locations map the depletion zone, hypocentral trends delineate faults (e.g., Stark, 1992), local earthquake tomography (LET) provides detailed 3-D structure, and focal mechanisms reveal reservoir processes.

The main objectives of the current experiment were to obtain (1) high-quality 3-D structural images of the reservoir volume using LET, and (2) accurate moment tensors. Although several seismic networks had been deployed in the area prior to our experiment, none could supply the data needed to meet these objectives, which require recordings from about 15 high-quality digital three-component stations encompassing the reservoir. For this reason we deployed a purpose-designed temporary network in 1991.

A large set of well-distributed earthquakes was recorded that reveal a striking negative V_P/V_S anomaly that probably defines the reservoir depletion zone and is evolving with time. The occurrence of nonshear earthquakes was confirmed. The

Manuscript received by the Editor May 13, 1997; revised manuscript received April 21, 1998.
*Amoco (U.K.), Exploration Co., Amoco House, Westgate, London W5 1XL, United Kingdom. E-mail: rossac@bp.com.
‡Department of Geological Sciences, University of Durham, Science Laboratories, South Road, Durham DH1 3LE, United Kingdom. E-mail: g.r.foulger@durham.ac.uk.
**U.S. Geological Survey, 345 Middlefield Road, MA 977, Menlo Park, California 94025. E-mail: julian@andreas.wr.usgs.gov.

results of the tomography studies have already been reported (Julian et al., 1996; Ross, 1996; Foulger et al., 1997) as has a preliminary summary of a few moment tensor results (Ross et al., 1996). This paper discusses the correlation of production and seismicity, and presents details of the full suite of 30 moment tensors obtained.

GEOLOGY AND GEOPHYSICS OF THE GEYSERS

The Geysers area is comprised of sedimentary and metamorphic rocks of the Franciscan Complex and Clear Lake volcanics (Hearn et al., 1981). It is intruded by the "felsite" batholith which is thought to be ~1 million years old (Hulen and Nielson, 1993). High-angle faults truncated by younger thrust faults criss-cross the area, in addition to strike-slip and normal faults of the current transform regime (Thompson, 1992). The steam reservoir underlies impermeable caprock, the base of which is 1.1–3.3 km below the surface, and occupies Franciscan rocks and the upper part of the felsite batholith.

The temperature of the main reservoir is about 235°C, and a small "high-temperature" reservoir with temperatures up to 342°C underlies this in the northwest of the area (e.g., Truesdale et al., 1993). Steam pressure was ~3.5 MPa (~500 psi) prior to large-scale exploitation, but is now as low as 1.5 MPa (~220 psi) in places (Barker et al., 1992). The reservoir fluid is stored as interstitial water which flashes to steam during its ascent up the boreholes.

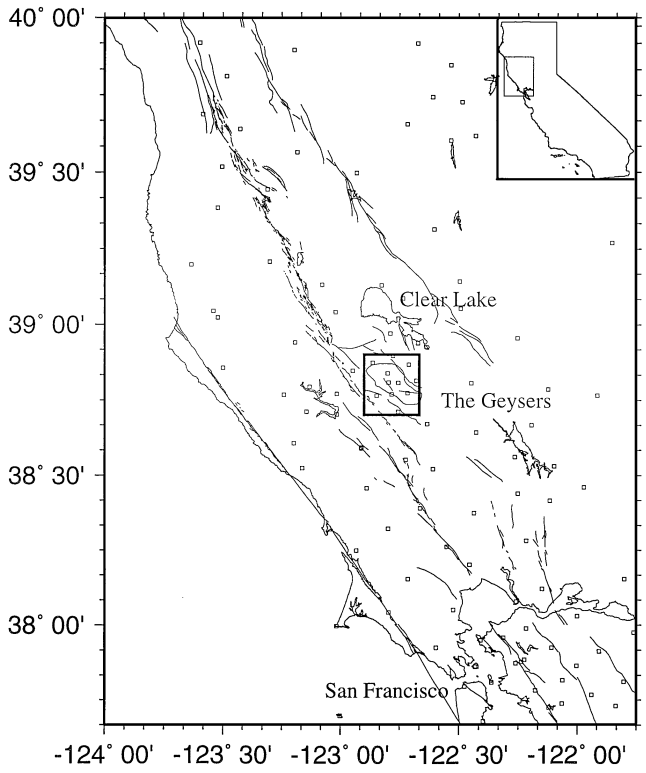

FIG. 1. Map showing the location of The Geysers area in California. The Geysers area is enclosed by a box, and the steam production zone is outlined inside this box. Squares are NCSN seismic stations; thin lines are faults; inset is regional location of main map.

An extensive negative Bouguer gravity anomaly with an amplitude of up to −25 mGal encompasses the area (Isherwood, 1981). Teleseismic *P*-waves recorded in the area are delayed by up to 1 s (Iyer et al., 1981). These observations are consistent with a body of partial melt at mid-crustal depths underlying the whole area (e.g., Blakely and Stanley, 1993). Geodetic surveying indicates volumetric contraction (Lofgren, 1981) with subsidence of up to 3 cm/year and horizontal contraction of up to 2 cm/year in the early times of reservoir exploitation. Truesdale et al. (1993) suggest that the heat source is a cooling magma body at 7–10 km depth that is younger than 0.1 Ma.

Steam reservoirs are very rare and require special circumstances to exist which are not well understood. Exploitation of The Geysers began in the 1860s, and steam was first used to generate electricity in 1922 when 1 kW was produced. Production has now risen to such a level that The Geysers currently supplies 6% of northern California's electrical power. Spent steam is either vented into the atmosphere or condensed and reinjected, which, in addition to mitigating fluid depletion, provides a convenient way of disposing of corrosive condensate. However, there is a large net fluid loss, and the natural recharge rate is essentially zero.

In an effort to mitigate reservoir depletion, two pipelines are currently under construction to transport partially treated sewage ("gray water") from nearby towns for injection. The first of these came on line in spring 1997. These projects may increase the amount of water injected into the whole reservoir by 30%. The heat in the reservoir is largely stored in the rock itself rather than the fluid, and it is depletion of the fluid that is exhausting the reservoir. If this problem could be solved, the lifetime of the reservoir could be extended.

SEISMIC MONITORING AND SEISMICITY AT THE GEYSERS

The earliest earthquake measurements at The Geysers were made in 1968, when six temporary seismometers were deployed in the southeast Geysers for five days (Lange and Westphal, 1969). Small temporary networks were again deployed in 1971 (Hamilton and Muffler, 1972) and 1982 (O'Connell, 1986). Continuous monitoring by a permanent network began in 1975 when the US Geological Survey (USGS) Northern California Seismic Network (NCSN) was extended into The Geysers. There are now 8 NCSN stations within 25 km of The Geysers. In 1985, the Unocal-NEC-Thermal (UNT) partnership established a dense analog network specifically to monitor earthquakes in the reservoir. Small digital three-component networks have been run in the northwest and southeast Geysers intermittently since 1988 and 1992, respectively (e.g., Kirkpatrick et al., 1995).

NCSN stations mostly contain vertical-component, 1-Hz sensors that transmit analog signals by microwave link to the San Francisco Bay area. *P*-phase arrivals are automatically picked in real time, and hypocenters and magnitudes calculated. Up to 40 stations regularly contribute data for earthquakes occurring at The Geysers. The NCSN location threshold for events in The Geysers decreased from magnitude 1.2 in 1975 to 0.5 from 1981 onwards (Eberhart-Phillips and Oppenheimer, 1984).

The UNT network currently includes 22 stations, seven of which are three-component and several of which are in boreholes (Figure 2). Analog data are transmitted via

telecommunication lines, digitised at 100 samples per second, and hypocenters and magnitudes automatically calculated. The detection threshold is approximately magnitude 0.2.

Seismic activity in The Geysers has increased steadily from the early 1970s to the present (Figure 3). A particularly rapid increase is evident between 1981 and 1989, along with an expansion of the seismogenic volume. Clustering becomes conspicuous in the 1990s. Until 1989, the northwest and southeast Geysers were largely aseismic, but between 1989 and 1995 activity expanded into these areas also. Some volumes within the central Geysers remained aseismic throughout the whole period, for example, a horizontal layer in the depth range ~2.5 to 3.0 km below sea level (bsl), and an area known as the "dead zone" in the center of the reservoir (M. A. Stark, personal communication, 1944).

It is clear that seismicity at The Geysers is correlated with industrial exploitation and that production rate correlates closely with seismic rate (Figure 4). An excess of earthquakes appears to have occurred recently, perhaps because of increased reinjection, which is thought to induce up to 50% of the earthquakes (Stark, 1992; Romero et al., 1994; Kirkpatrick et al., 1995). Many theories have been advanced for the mechanism of induction, but the most likely explanation is that they occur as the reservoir rocks are strained in response to the removal of large volumes of the pore fluid (e.g., Majer and McEvilly, 1979).

DATA ACQUISITION

Despite the fact that The Geysers is highly seismically active and numerous networks have been operated there, digital three-component data from a calibrated network encompassing the whole reservoir were unavailable in 1991. We thus installed a temporary network of 15 stations for the month of April 1991 (Figure 2). The sensors were Mark Products model L22D 2-Hz, three-component instruments with natural frequencies of 2 Hz. They were plastered onto bedrock in shallow pits. Data digitised at 100 sps were recorded by Reftek model 72A data loggers and recorded continuously in order to avoid the substantial loss of data that invariably accompanies the use of event-detection algorithms. All the station locations, including those of the UNT stations, were determined by differential GPS, and timing was achieved using the Omega and WWVB time signals and master clocks.

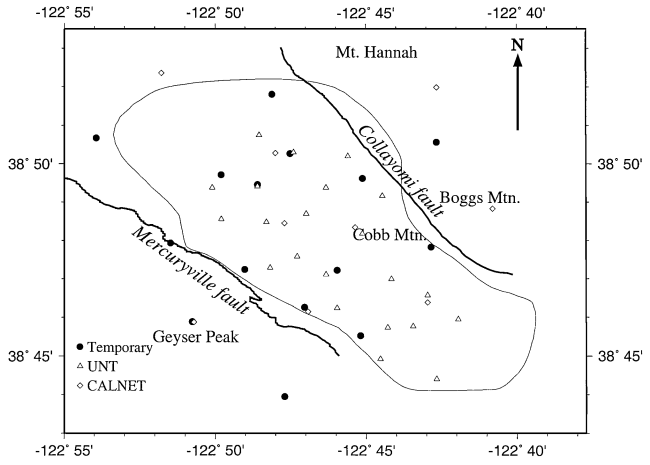

FIG. 2. Map of The Geysers geothermal area showing stations of the NCSN and UNT permanent networks, and the temporary network deployed in April 1991. Outlined area is steam production zone.

The stations were sited to achieve uniform distribution over the focal sphere for a hypothetical earthquake at about 3 km bsl in the middle of the reservoir. The best crustal model for The Geysers available (Eberhart-Phillips and Oppenheimer, 1984) was used to calculate optimum locations for the stations. These had to be amended in practice because of logistics and the very complicated land ownership situation at The Geysers.

We recorded a total of 18 gigabytes of continuous data from which 3900 earthquakes were extracted. Our data were supplemented by data from the UNT network for the same time period. This network is not calibrated, and the polarities of the vertical instruments, along with the orientations of the horizontal instruments, are unknown. Therefore, the data could only be used for arrival-time information, which contributed to hypocentral locations. Data from NCSN were also used, and the final data set included data from 90 vertical and 22 horizontal instruments.

3-D STRUCTURE

The main results of the tomographic inversion are reported by Julian et al. (1996), and the theory and method are described by Thurber (1983) and Eberhart-Phillips (1993). Only a brief summary of the results will be given here. As a result of the very large numbers and good distribution of stations and earthquakes available, very high-quality 3-D V_P and V_P/V_S structures were imaged. The best 1-D model for the area was calculated using program *velest* which simultaneously inverts earthquake arrival times for 1-D structure and hypocenters (Kissling et al., 1994) (Table 1). The best average estimate of V_P/V_S for the area, 1.74, was obtained from Wadati diagrams.

Considerable heterogeneity was detected. V_P varies by up to about 30% from the average in each layer with low wave-speed anomalies prominent at shallow depths and high wave-speed anomalies prominent at depths >2 km bsl. A strong velocity change occurs across the Collayomi fault zone. Some of the V_P anomalies correlate with certain geological features, but they do not correlate with the steam reservoir.

The most remarkable anomaly occurs in V_P/V_S. This parameter usually varies little, but at The Geysers a striking low V_P/V_S anomaly of up to about 10% correlates very closely with the steam reservoir at all depths. Moreover, this anomaly became about 4% stronger between 1991 and 1994 in areas where pore pressure was dropping most rapidly (Foulger et al., 1997). V_P/V_S is comparatively insensitive to variations in mineralogy and porosity in this area, but does depend (through V_P) upon the compressibility of the pore phase, and thus is sensitive to the difference between liquid and gaseous pore fluid and to pore pressure when the pore fluid is a gas. Julian et al. (1996) gave a simplified quantitative analysis of this effect at The Geysers, based on Reuss-average estimates of the effective bulk moduli of rocks, and concluded that the observed anomaly is roughly compatible with the expected effect of replacing liquid pore water with vapor. This analysis does not, however, explain why the anomaly is not evident in the V_P field alone, and Julian et al. (1996) hypothesized that the steam reservoir must be lithologically different from its surroundings. Recent acoustic

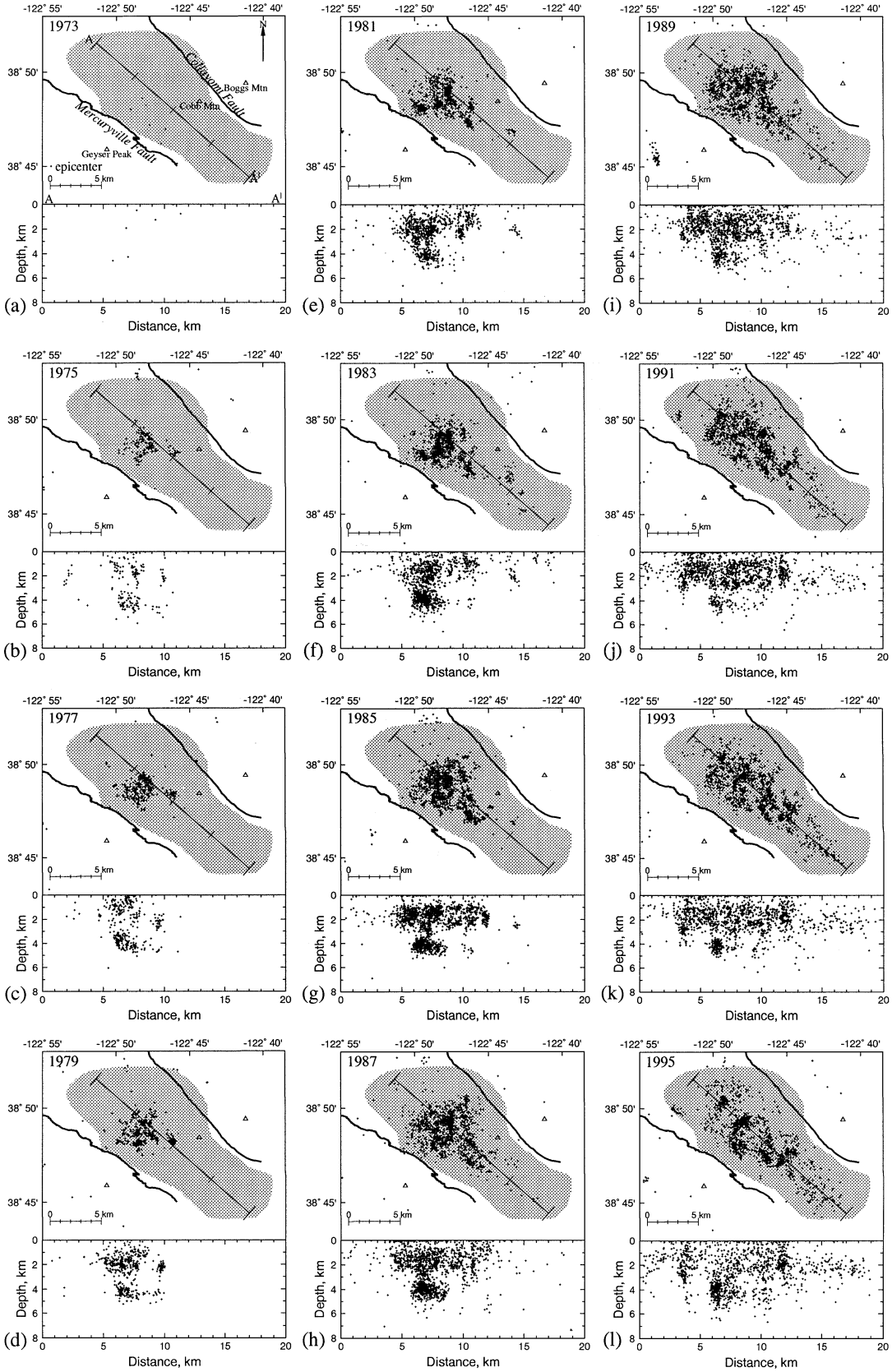

FIG. 3. Maps of seismicity at The Geysers at biannual intervals from 1973 to 1995. NCSN locations for earthquakes with magnitudes >1.2 are shown. Earthquakes located within the steam field are presented on the cross sections.

measurements made by Boitnott and Boyd (1996) on core samples from The Geysers cast light on the nature of this difference. They found that drying increases the rigidity modulus μ through a chemical-mechanical effect (the "spaghetti" effect), thus raising V_S and adding to the negative V_P/V_S anomaly. This effect increases V_P (because V_P also depends on μ) and may explain the absence of a clear V_P anomaly. It is not yet clear, however, how widespread such effects of drying upon mineral elasticity may be.

The earthquakes were relocated using these 3-D structural models and the program *qloc3d* which locates events in a 3-D structure using bending ray tracing (Julian and Gubbins, 1977). The average horizontal and vertical change in locations from the 1-D to the 3-D model were 0.34 and 0.29 km, respectively, with maximum movements of 2.97 and 2.54 km, respectively. Relocated earthquakes tended to cluster more, and the final *P*- and *S*-wave traveltime residuals were 0.041 s and 0.074 s, respectively. The locations obtained using the 3-D model provided highly accurate positions of the stations on the focal sphere, and thereby enhanced the quality of the moment tensors subsequently derived.

These earthquake locations (Figures 5 and 6) are more accurate than automatic NCSN or UNT locations. A layer that is almost aseismic <0.4 km in thickness underlies The Geysers at about 3.0 km bsl, dividing the earthquakes into two vertically distinct zones (Figure 6). Furthermore, almost no events occur deeper than 4.0 km bsl. This contrasts with locations, for example, from the NCSN catalog, which shows deeper events. This suggests that the base of the seismogenic volume may be shallower than hitherto suggested by locations obtained automatically using 1-D models.

Table 1. The best one-dimensional crustal model for The Geysers area (Ross, 1996).

Depth bsl (km)	*P*-wave speed (km/s)
−2.0	2.47
−1.0	3.52
0.0	4.33
1.0	4.53
2.0	5.02
3.0	5.08
4.0	5.21
6.0	5.75
7.0	5.83

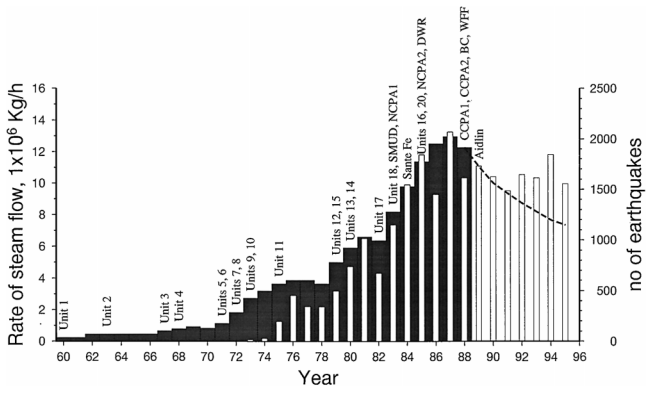

FIG. 4. Average steam flow rate per hour between 1960 and 1988 (black columns) (modified from Barker et al., 1992). The dashed line indicates the projected steam flow rate from 1989 to 1995 (modified from Williamson, 1992). The white columns indicate the number of earthquakes with magnitudes >1.2 recorded in The Geysers by NCSN between 1973 and 1995. The installation times of electrical-power generating units are indicated.

EARTHQUAKE MOMENT TENSORS

Early attempts to derive focal mechanisms

Using NCSN data, computer-derived fault-plane solutions were calculated for ~400 earthquakes at The Geysers by Oppenheimer (1986). The earthquakes were constrained to

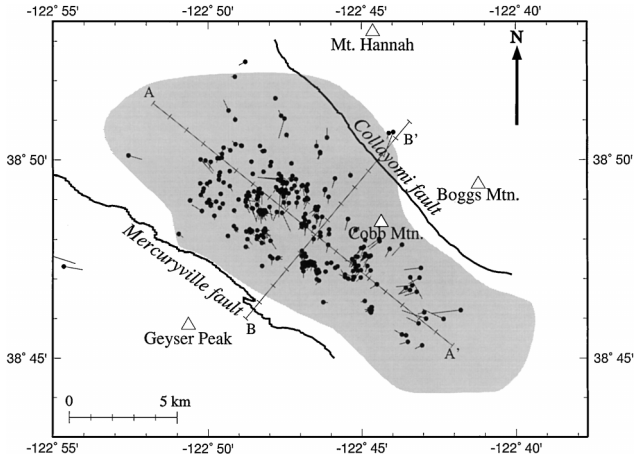

FIG. 5. Changes to epicenters located with the regional 1-D V_P model when the final 3-D V_P and V_S models are used. Black dots are the 3-D locations; a line connects them to the 1-D locations. A-A' and B-B' are the lines of cross-section used in Figure 6.

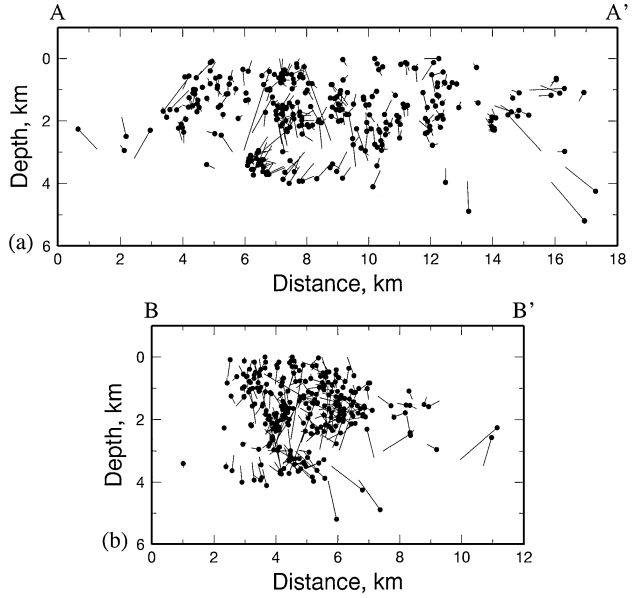

FIG. 6. (a) Northwest-southeast and (b) southwest-northeast cross-sections showing changes between hypocenters located with the regional 1-D and the final 3-D wave-speed models. Symbol convention is as in Figure 5.

have double-couple source mechanisms. Wide variations in the type of solution were obtained for spatially close events, and little consistency in fault-plane orientation was detected.

As a result of a large number of recent reports of well-constrained non-double-couple earthquake mechanisms, it is now generally accepted that solely shear motion at the source is not a fundamental property of all earthquakes (Julian et al., 1997b; Miller et al., 1997). Many well-constrained volcanic and geothermal earthquakes in particular have nonshear mechanisms, often with substantial volumetric components (e.g., Foulger, 1988b; Shimizu et al., 1988; Foulger et al., 1989; Julian et al., 1997b). O'Connell and Johnson (1988) studied a few earthquakes from The Geysers using waveform inversion techniques. They identified one event that had a non-double-couple (non-DC) component in the source mechanism but attributed this to error. Julian et al. (1993) noted that many of the *P*-wave polarity plots presented by Oppenheimer (1986) were dominated by arrivals of the same polarity and suggested that 10–20% of the earthquakes at The Geysers may have non-DC mechanisms. Kirkpatrick et al. (1996) confirmed this observation for earthquakes from the southeast Geysers by inverting polarities and amplitudes using a method not explained in detail.

Calculation of earthquake moment tensors

Digital data from the temporary network and NCSN were combined to calculate general moment tensors using both *P*- and *S*-wave polarities and *P*:*S* amplitude ratios. The linear-programming method was used. This method and its application is described in detail by Julian and Foulger (1996).

P-, *SH*-, and *SV*-waves were used, the *S*-phases being measured from rotated seismograms (Figure 7a). All seismograms were filtered with a low-pass corner frequency of 5 Hz (Figure 7b). Measured amplitudes were corrected for free-surface effects and attenuation (Miller, 1996; Ross et al., 1996). A value of $Q_P \cong 60$ has been obtained from attenuation studies of The Geysers (Zucca et al., 1993), but Q_S has not been investigated. In this study, a range of values for Q_S was tried, ranging from 5 to 500. The results were found to be insensitive to Q_S, and a value of $Q_S \cong 84$ was chosen, corresponding to $Q_P/Q_S = 0.71$.

The method requires that amplitudes and amplitude ratios are expressed in terms of bounding values, which reflect the errors in the observations. The errors due to noise were estimated by measuring the amplitude of noise prior to the *P*-wave, and of *P* coda prior to the *S*-wave arrivals on each seismogram. The error due to unmodeled wave-propagation effects was estimated

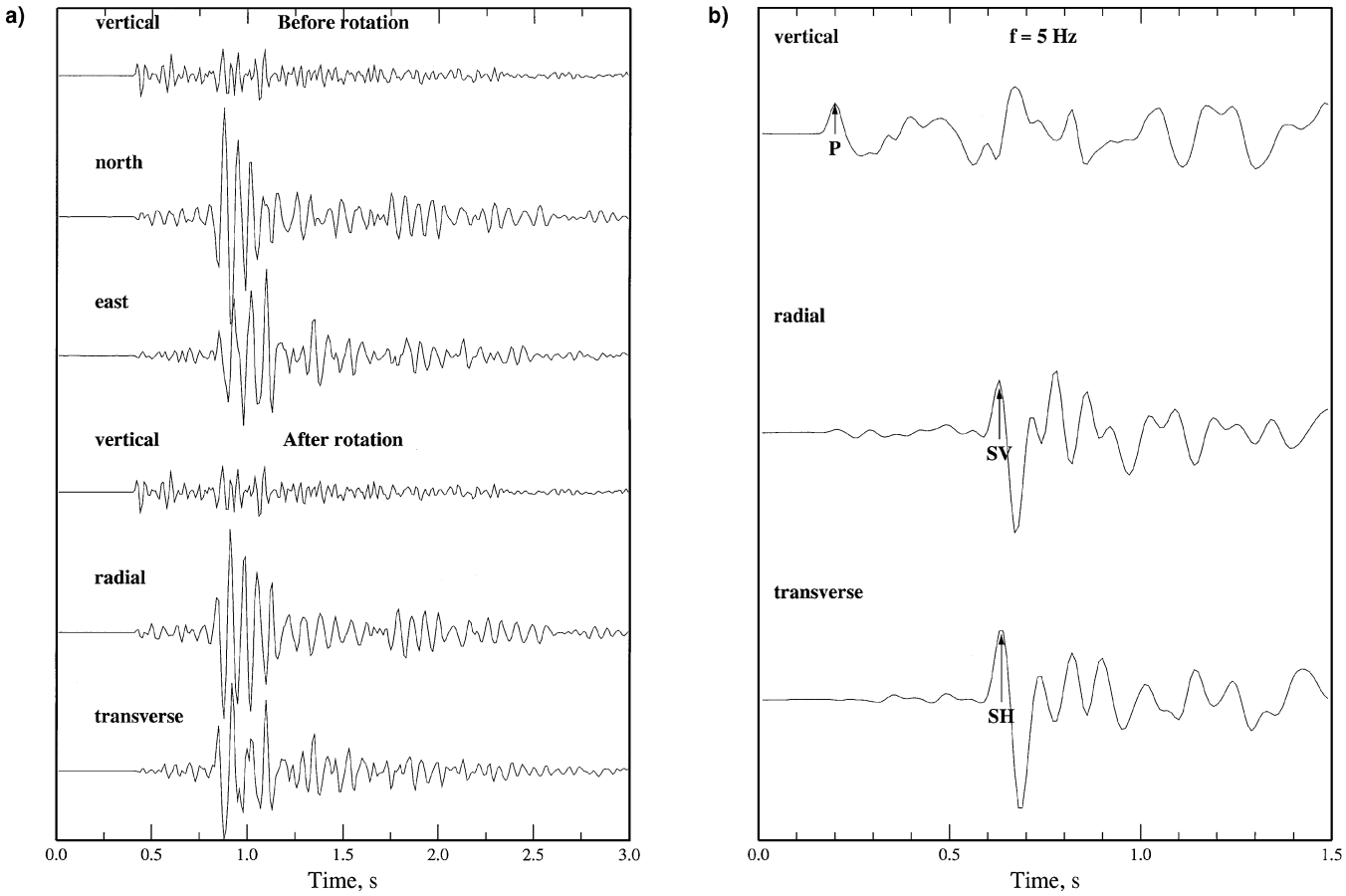

FIG. 7. (a) Examples of unrotated and rotated seismograms. The north component is aligned to true north. The bottom two traces show the rotated radial and transverse horizontal components. The *SH* and *SV* arrivals are separated on the rotated traces. (b) The rotated traces shown in (a) after low-pass filtering using a three-pole Butterworth filter with a corner frequency of 5 Hz. The vertical trace is magnified vertically by a factor of three relative to the radial and transverse components.

empirically by inverting for the moment tensors for several earthquakes using different estimates of this error and selecting the value that resulted in about 50% of the events yielding solutions compatible with all the data within the estimated errors. This study suggested that 40% was an appropriate value.

To test at which point moment tensors become poorly constrained as a result of insufficient data, a series of inversions was performed on a well-constrained event which has 11 *P*- and 10 *SH*-wave polarity observations (Figure 8). Stations were progressively eliminated from the dataset while maintaining an even distribution on the focal sphere. The resultant solutions show surprising consistency, even when the data set is impoverished to three amplitude ratios, and four *P*-wave and three *S*-wave polarity observations. The orientations of the principal axes are successfully recovered in each inversion. The superior resolving power of the method over inversions using *P*-polarities only was also demonstrated by Miller (1996), who showed that moment tensors determined using 10 three-component stations were superior to those obtained with 27 one-component stations.

Moment tensors were calculated for 30 of the best-recorded earthquakes. The method used here delivers very high quality results, but is not automatic. For this reason, the data set is limited. Most of the earthquakes were located in the central part of the production zone at depths of 0.78 to 3.98 km bsl (Figure 9). Those at depths ≥2 km bsl have the best focal sphere distribution, and up to 27 polarity observations and 10 amplitude ratios were available (Figures 10 and 11).

The "source-type plot" (Hudson et al., 1989) (Figure 11) displays the relative magnitudes of the three principal moments of the moment tensor, providing a description of the source type that is independent of orientation. The plot is scaled so that

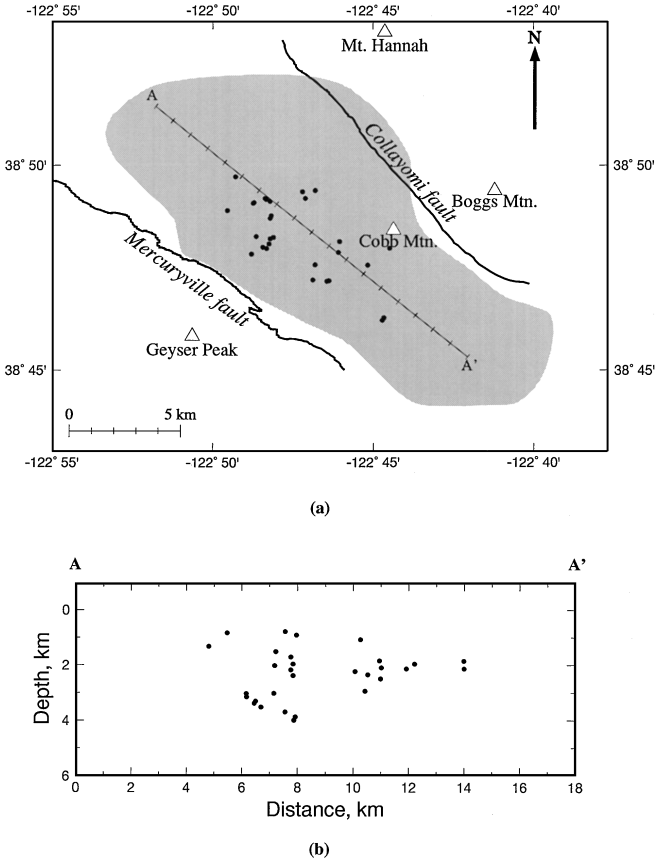

FIG. 9. (a) Map and (b) cross-section of The Geysers showing the locations of the 30 events for which moment tensors were derived.

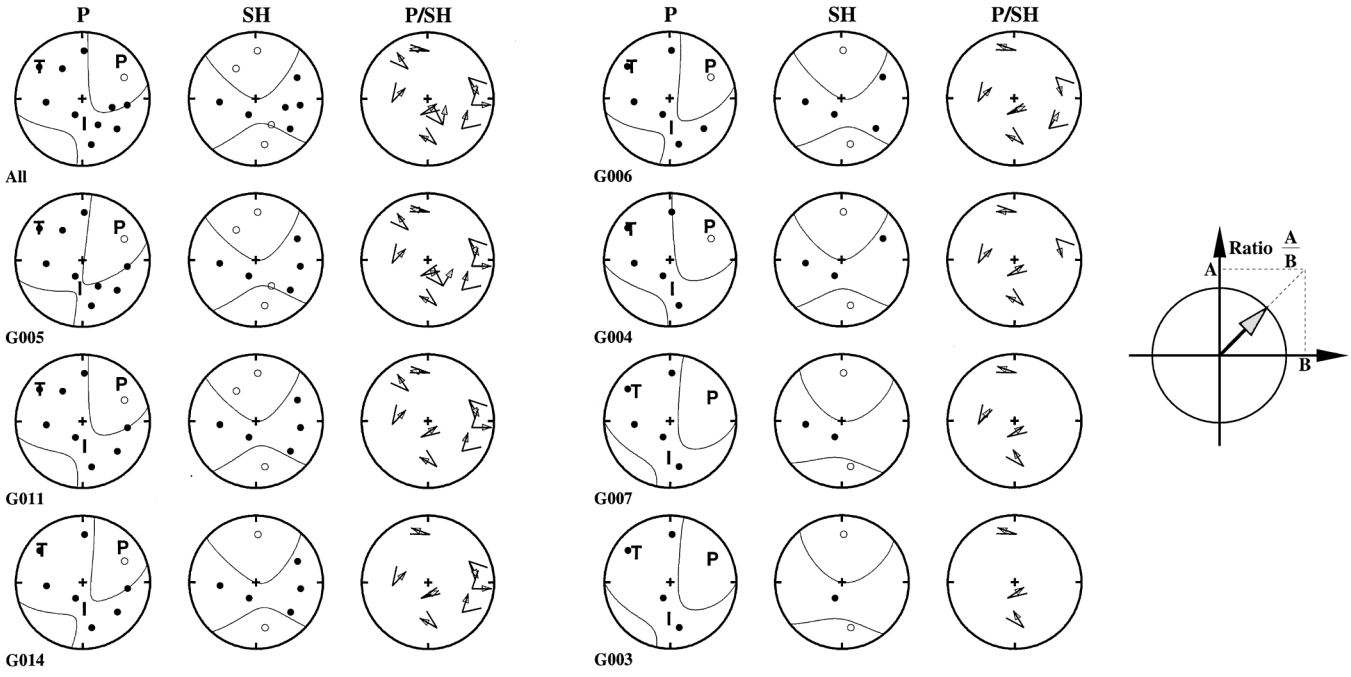

FIG. 8. Focal mechanism solutions for a well-recorded event determined initially with all available polarity and amplitude data, and subsequently discarding stations one by one. Black dots are compressional *P* or clockwise *S* motion; arrows are *P:SH* amplitude ratios depicted using the convention illustrated in the key at right; pairs of lines are error bounds of amplitude ratios.

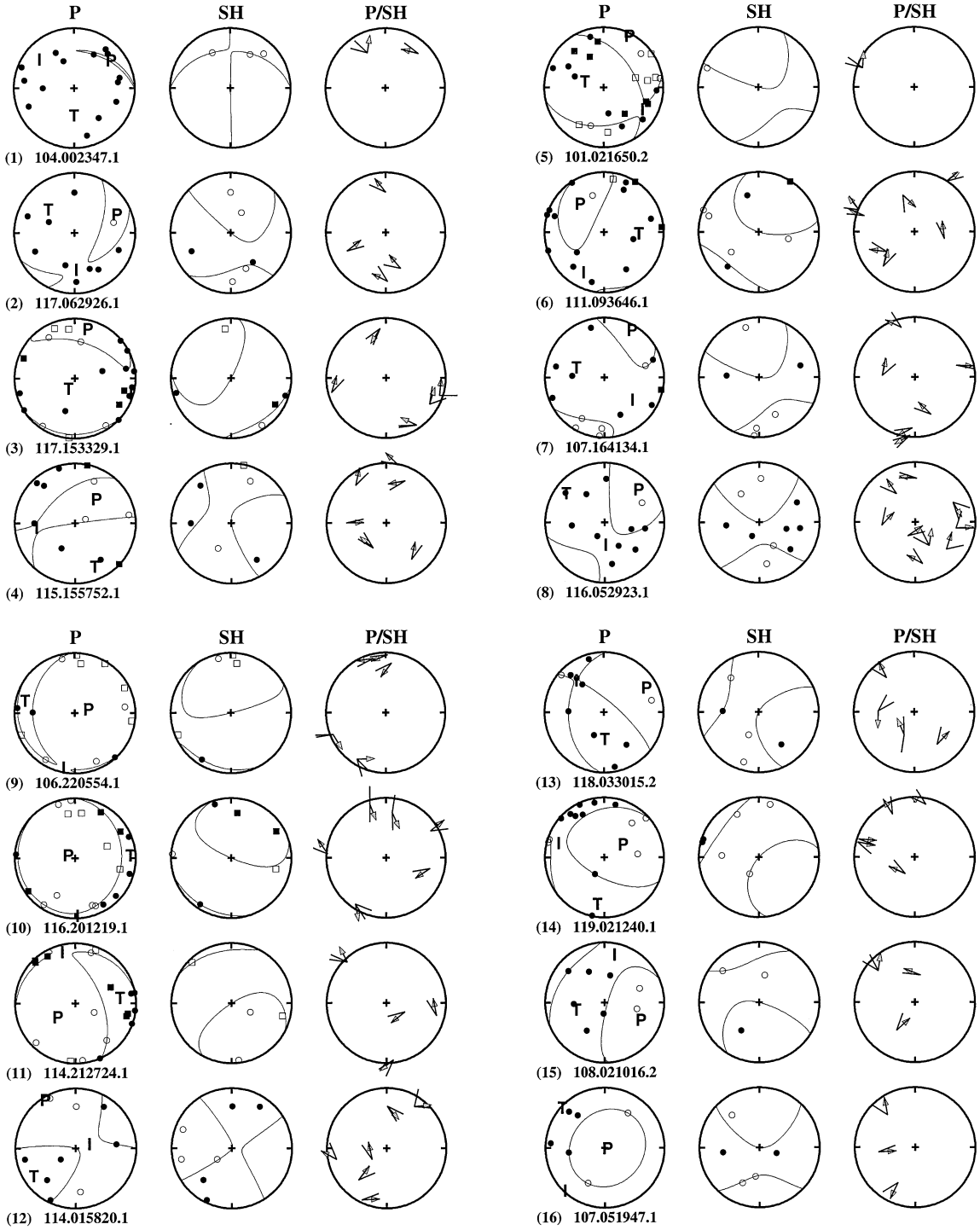

FIG. 10. Focal mechanism solutions of 30 earthquakes. Symbols as used in Figure 8. Each earthquake is labeled by the day and time of the first sample of the data file.

the probability density of all source types is uniform throughout the plot, assuming that the principal moments have a uniform distribution. The plot displays two quantities,

$$T \stackrel{\text{def}}{=} \frac{2m'_1}{|m'_3|}$$

and

$$k \stackrel{\text{def}}{=} \frac{m^{(v)}}{|m^{(v)}| + |m'_3|},$$

where m'_1, m'_2, and m'_3 are the principal moments of the deviatoric moment tensor arranged so that $|m'_1| \le |m'_2| \le |m'_3|$, and

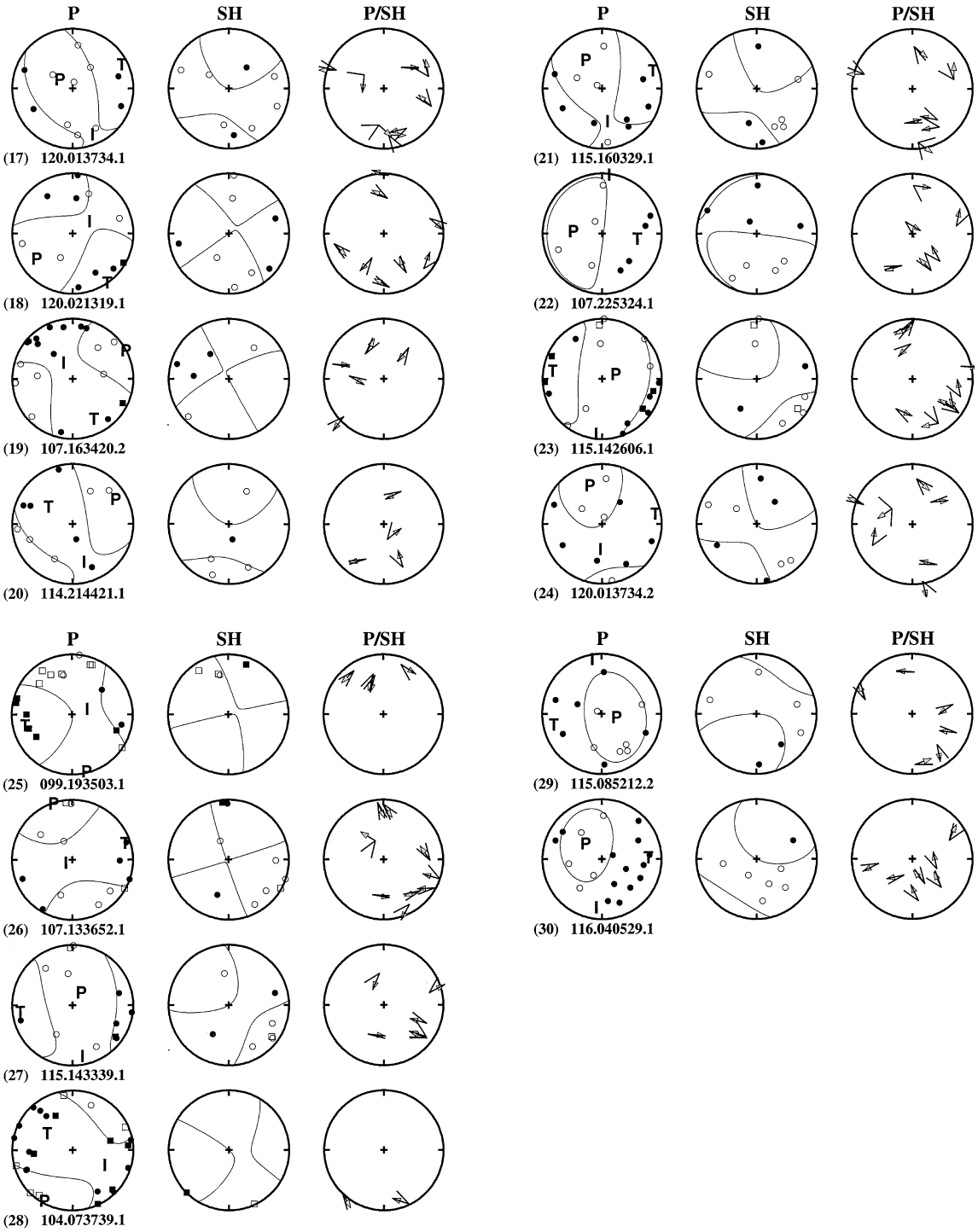

FIG. 10. (*Continued.*)

$m^{(v)} = Tr(M)/3$ is the volumetric component. T lies in the range 1 to −1, and describes the departure of the deviatoric component from a double couple (DC), and forms the horizontal axis in Figure 11. For compensated linear vector dipole sources (CLVDs), T is ±1. The parameter k measures the relative volumetric change, with $-1 \le k \le 1$, and forms the vertical axis in Figure 11. For deviatoric mechanisms, including DCs and CLVDs, $k = 0$. For a DC, $T = k = 0$. Our data constrain T more poorly than k. For well-constrained events, the scatter in the value of T obtained after eliminating a few data is typically of the order of ±0.2, compared with ±0.05 for k (Miller, 1996).

Notwithstanding the effects of errors, our results show considerable variation. The final results presented here represent a larger data set and supercede the preliminary results presented by Ross et al. (1996). Only about 30% of mechanisms are close to deviatoric, and the rest have significant positive or negative volumetric components with approximately equal numbers of each (Figure 11). About 50% of the earthquakes have volumetric components ≥20% of the total moment, and the volumetric components of 5 events exceed 30%. The events occupy a broad zone on the source-type plot that extends from the DC locus to the ±Dipole loci. None of the events are close to the ±Crack loci. One earthquake has almost a +Dipole moment tensor, and two others have moment tensors very close to a −Dipole. Of particular interest is event 1 (Figure 10), which has only compressional first motions. The nodal lines define what is probably an insignificant area of predicted dilational radiation, and the *S*-waves recorded for this event were very small.

The sizes of the implosive and −CLVD component correlate with depth, with the larger components tending to accompany the shallower earthquakes (Figure 12). No correlation with depth is apparent for the explosive and +CLVD components, however. The moment magnitudes are also independent of the size of the volumetric and CLVD components (Figure 12). There appears to be no spatial or temporal dependence on the type of mechanism either. For example, events 17 and 24 (Figure 10) were separated by 30 s in time and occurred at almost the same location. Both are well constrained, but they have rather different moment tensors, although the P- and T-axes have similar orientations.

The orientations of the principal axes for whole data set show considerable variation (Figure 13). The P-axes mostly have trends ranging from northeast to northwest and plunges ranging from subhorizontal to vertical. The trends of the T-axes are even more variable; neither show evidence of depth dependence (Figure 14).

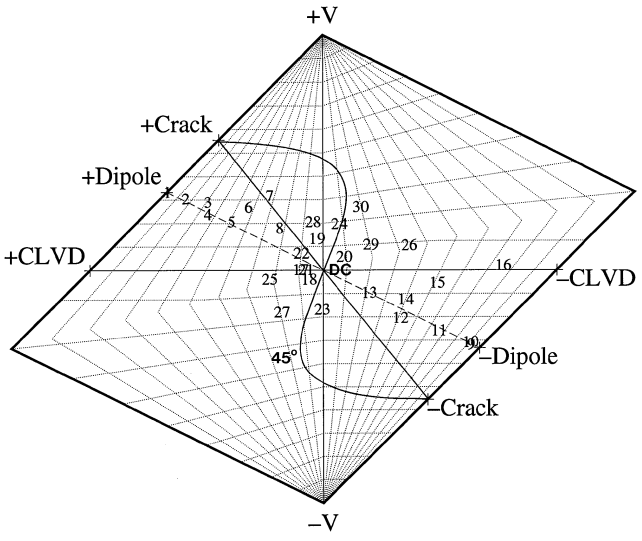

FIG. 11. Source-type plot showing the 30 earthquakes studied. ±Crack are opening/closing tensile crack; ±Dipole are force dipole with force directed outward/inward; ±CLVD are compensated linear vector dipole with dominant pole directed outward/inward. The area enclosed by the line joining the ±Crack points and the curve labeled 45° is the locus of tensile crack + shear crack combinations where the T-axis of the tensile crack is within 45° of the P-T plane of the shear crack. Tensile/shear crack combinations with different geometries are unlikely as one or both components would be extremely inconsistent with the ambient stress field.

DISCUSSION

Industrially induced environmental change at The Geysers

In the early days of commercial exploitation of The Geysers, operators expected a limitless future for the resource and invested little in research aimed at understanding the reservoir or processes within it. Development grew at a moderate rate until 1980, when a number of factors, including government incentives encouraging the use of alternative energy resources, resulted in an influx of new investors and developers. Against the advice of independent experts, who saw overdevelopment of the resource a real possibility, growth in new capacity almost doubled annually. By 1989, The Geysers had an installed generating capacity of 2043 MW. Decline in steam pressure became significant in 1987 and is so serious that today the actual electrical power generated is considerably less than the installed capacity. Better resource management, involving a sensible research program, could have predicted the impending decline and perhaps defined ways of mitigating it. If production had

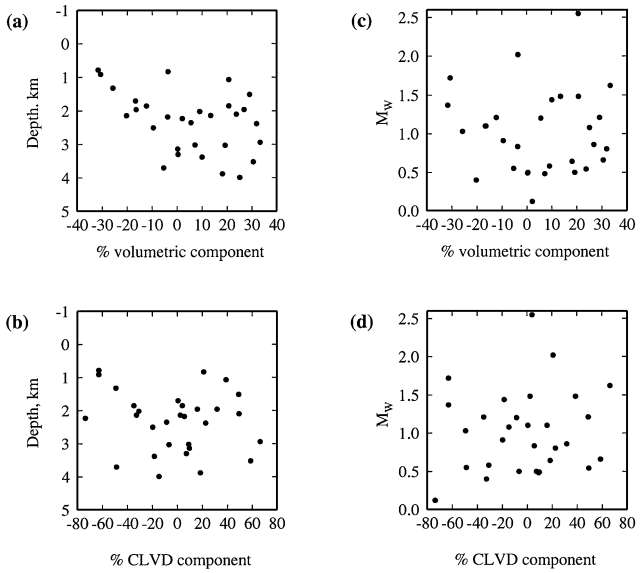

FIG. 12. (a) and (b) Variation of the volumetric and CLVD components of the 30 moment tensors with depth; (c) and (d) variation of the volumetric and CLVD components with moment magnitude.

been maintained at the 1980 level of 943 MW, all the generating plants installed, which numbered 14 then, might be operating today at full strength, and a lot of money would have been saved (Kerr, 1991).

Today, operators are urgently seeking methods to arrest the pressure decline, and to this end much proprietary information has been released to the scientific community. Condensate reinjection has slowed the decline of wells, with the steam temperature remaining steady even after prolonged periods of injection of 20–30°C fluid (Enedy et al., 1992). Gray water will be injected at <10°C, however, and it remains to be seen whether the reservoir can sustain large, long-term injections of fluid this cold, and whether difficulties will arise from more frequent water breakthroughs at the base of production wells and temperature decline.

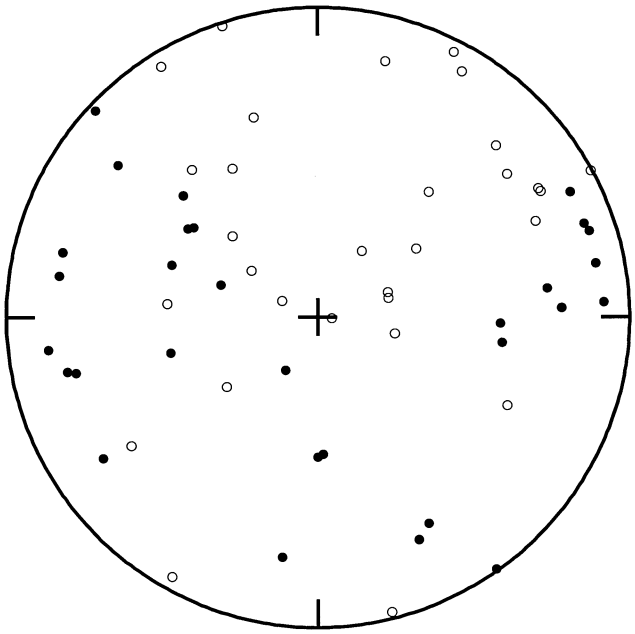

FIG. 13. Equal-area upper hemisphere projection showing the *P*- (open circles) and *T*-axis (solid dots) orientations for the 30 earthquakes studied.

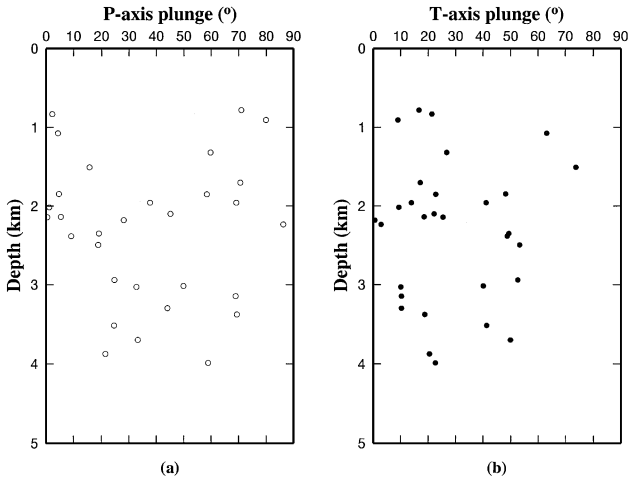

FIG. 14. Plunges of (a) *P*-axes, and (b) *T*-axes versus depth for the 30 earthquakes studied.

Of increasing importance is the issue of industrially induced seismicity. Fluid injection may induce larger earthquakes than production, and progressive volume contraction of the reservoir is loading nearby tectonic faults. Greatly increasing the level of injection may exacerbate these problems to a significant but as yet unquantified degree.

Nonshear earthquake focal mechanisms

That earthquakes at The Geysers have nonshear focal mechanisms is convincingly shown by this study, and the suite of 30 well-constrained solutions is sufficient to show their distribution in source-type parameter space. The detection of abundant implosive earthquakes in a geothermal area is a rare finding; only one other case has been reported, from the Krafla-Namafjall geothermal area, Iceland (Foulger et al., 1989; Arnott and Foulger, 1994). Those earthquakes were also beneath industrial-well fields, as was a single implosive earthquake recently reported from the Hengill-Grensdalur area, Iceland (Miller, 1996; Julian et al., 1997a). Such implosive mechanisms must result from the collapse of cavities at depth in the Earth, and this finding is evidence that such cavities exist at The Geysers. This is supported by reports that drill holes at The Geysers often intersect substantial cavities (B. Cumming, personal communication, 1997).

The events cover a broad range in parameter space (Figure 11) with volumetric components up to about 30% of the total moment and CLVD components up to 100% of the deviatoric component. It is particularly interesting to note that several events are almost exactly dipoles (±Dipole: Figure 11, events 1, 9, and 10) but no events are close to tensile cracks (±Crack).

A combination of an opening/closing crack and a shear crack is an intuitive model for these events, but it cannot explain all the observations. The locus of all such sources with likely relative crack orientations is shown on the source-type plot in Figure 11. Although the errors in T are greater than in k (Miller, 1996), several well-constrained events (e.g., event 16) plot far from this locus. Ross et al. (1996) suggest that the sources may be explained by combinations of tensile cracks and DCs accompanied by fluid flow that partially compensates the seismic volumetric component. The observations are consistent with such a model, and where cracks open in the presence of high-temperature and pressure fluids, rapid flow into the new void, possibly accompanied by water flashing to steam, is to be expected. The reciprocal process would occur accompanying crack implosion.

Interpretation of the non-DC earthquakes at The Geysers depends heavily on whether the earthquakes are industrially induced or not. High rates of nonshear natural seismicity appear to be common in unexploited geothermal areas (e.g., the Hengill-Grensdalur area, Iceland; Julian et al., 1997). There is, however, strong evidence that the majority of earthquakes at The Geysers are industrially induced. In that case, the most obvious processes that might cause cavities to open and close are fluid injection and withdrawal. The removal of large volumes of fluid is known to cause substantial volumetric contraction (Lofgren, 1981). Whereas volumetric contraction in the vertical direction may be accommodated by surface subsidence, no free surface is available to take up contraction in the horizontal direction, which may thus be accommodated by crack

opening. Another possible explanation is that fluid reinjection forces cracks open. Cavity collapse, causing implosive earthquakes, could result from the removal of fluid causing a fall in the pore pressure supporting the cavity.

Although these arguments amount to attributing opposite results to the same processes, in the absence of a strong, systematic regional stress field, stress is likely to be highly variable locally. The scattered orientations of the *P*- and *T*-axes are evidence for this. High levels of natural seismicity would not be expected in the absence of a strong regional stress field, and this supports further the hypothesis that the earthquakes are industrially induced. This could also explain why induced earthquakes at The Geysers are not large. Similar findings have been reported from the Krafla geothermal area, Iceland (Arnott and Foulger, 1994).

The induction mechanism of explosive and implosive earthquakes could be studied by correlating earthquake source types spatially and temporally with exploitation activities. This aspect of the seismicity may be a potential discriminator as to the causative process inducing particular events. The locations of implosive and explosive earthquakes would be expected to correlate with production and injection wells, and also vary throughout the area. An analysis of a very large dataset from the southeast Geysers failed to reveal any correlation Kirkpatrick et al., 1996) and we found no such correlations in our small, field-wide dataset. However, further testing of this hypothesis is warranted with detailed analysis of a larger dataset.

Comparison with the Hengill-Grensdalur geothermal area, Iceland

A similar study to that reported here was conducted in the Hengill-Grensdalur geothermal area, Iceland (Foulger et al., 1995; Miller, 1996; Julian et al., 1997a). The main differences between the two geothermal areas are that the Hengill-Grensdalur area is water dominated, is largely unexploited except for a small field at Nesjavellir in the northwest corner, lies in the extensional tectonic stress regime of a spreading plate boundary, and generates a high level of naturally occurring seismicity.

Moment tensors were derived for 70 well-constrained earthquakes from this area. They show a very different distribution of source types from earthquakes from The Geysers (Figure 15, Table 2). Whereas about 25% of the earthquakes studied from The Geysers have significant implosive components, only one such earthquake was detected at the Hengill-Grensdalur area. That occurred directly below the Nesjavellir field (Table 2).

Explosive earthquakes, which must involve the opening of cavities, are, on the other hand, much more common in the Hengill-Grensdalur area. These were attributed to thermal contraction in the heat source as it cools in response to natural heat loss (Foulger, 1988a,b). Such a process cannot account for the explosive components at The Geysers, as the reservoir is not cooling (M. Stark, personal communication, 1994). There, volumetric contraction caused by the industrial removal of fluids or by injection are more likely explanations.

The maximum magnitude of the volumetric component is about the same for both areas (i.e., up to about 30% of the total moment), and this volumetric "ceiling" may have a physical meaning. The average volumetric component is larger for the Hengill-Grensdalur area, however. There, the majority of earthquakes have volumetric components of >20% of the total moment, whereas at The Geysers the majority have volumetric components of <20%.

Whereas the range of volumetric components observed at the two areas contrasts greatly, the CLVD components occupy a similar range, with about 30% of events from both areas having significant CLVD components up to about ±100% of the deviatoric component. However, whereas explosive earthquakes at the Hengill-Grensdalur area may have large CLVD components of either sign, no explosive earthquake from The Geysers has a large −CLVD component, and no implosive earthquake has a large +CLVD component. There is probably no one-to-one correspondence between the CLVD component and a physical source process, and so no straightforward interpretation of this observation is possible. The results of this work, however, do add to the debate of the physical meaning of nonshear earthquakes and whether they can provide information useful to geothermal resource exploitation.

Table 2. Comparison of source components resolved in earthquakes studied at The Geysers and the Hengill-Grensdalur geothermal areas. Earthquakes with volumetric components >10% of the total moment are categorized as "implosive" or "explosive," and earthquakes with CLVD components >20% of the deviatoric component are categorized as ±CLVD.

Type	The Geysers (% of 30 earthquakes)	Hengill-Grensdalur (% of 70 earthquakes)
Implosive	25	1
Explosive	40	85
Deviatoric	35	14
+CLVD	30	33
−CLVD	30	25

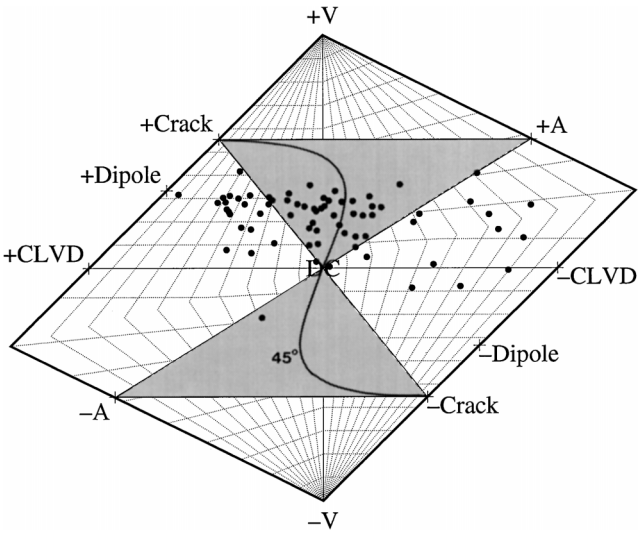

FIG. 15. Source-type plot showing the distribution of moment tensors (solid dots) for 70 earthquakes from the Hengill-Grensdalur geothermal area, Iceland (data from Miller, 1996). Shaded area is area where moment tensors may be explained as a combination of a DC and a tensile fault with any geometry. Other symbols as in Figure 11.

ACKNOWLEDGMENTS

We thank Mitchell Stark and the Unocal Corporation for assistance in deploying our network in 1991, data, and helpful discussions. IRIS-PASSCAL supplied the field equipment. Funding was provided by a USGS G. K. Gilbert fellowship, NERC Grant GR9/134, and a DENI studentship (AR). GMT (see Wessel and Smith, 1991) was used for figure preparation.

REFERENCES

Arnott, S. K., and Foulger, G. R., 1994, The Krafla spreading segment, Iceland : 2. The accretionary stress cycle and non-shear earthquake focal mechanisms: J. Geophys. Res., **99**, 23 826–23 842.

Barker, B. J., Gulati, M. S., Bryan, M. A., and Riedel, K. L., 1992, Geysers reservoir performance, *in* Stone, C., Ed., Monograph on The Geysers geothermal field: Geotherm. Res. Council Special Rep. **17**, 167–177.

Blakely, R. J., and Stanley, W. D., 1993, The Geysers magma chamber, California: Constraints from gravity data, density measurements, and well information, *in* Stone, C., Ed., The Geysers geothermal field: Geotherm . Res. Council Special Rep. **17**, 227–233.

Boitnott, G. N., and Boyd, P. J., 1996, Permeability, electrical impedance, and acoustic velocities on reservoir rocks from The Geysers geothermal field: Proc., 21st Workshop on Geotherm. Reservoir Engineering, 343–350.

Eberhart-Phillips, D., 1993., Local tomography: earthquake source regions, *in* Iyer, H. M., and Hirahara, K., Eds., Seismic tomography: Theory and practice: Chapman and Hall, 613–643.

Eberhart-Phillips, D., and Oppenheimer, D. H., 1984, Induced seismicity in The Geysers geothermal area, California: J. Geophys. Res., **89**, 1191–1207.

Enedy, S. L., Enedy, K. L., and Maney, J., 1992, Reservoir response to injection in the southwest Geysers, *in* Stone, C., Ed., Monograph on The Geysers geothermal field: Geotherm. Res. Council Special Rep. **17**, 211–219.

Foulger, G., l988a, The Hengill triple junction, southwest Iceland: 1. Tectonic structure and the spatial and temporal distribution of local earthquakes: J. Geophys. Res., **93**, 13 493–13 506.

———l988b, The Hengill triple junction, southwest Iceland: 2. Anomalous earthquake focal mechanisms and implications for process within the geothermal reservoir and at accretionary plate boundaries: J. Geophys. Res., **93**, 13 507–13 523.

Foulger, G. R., Grant, C. C., Julian, B. R., and Ross, A., 1997, Tomographic imaging of progressive pore-fluid depletion of The Geysers geothermal reservoir, California: Geophys. Res. Lett., **24**, 135–137.

Foulger, G. R., Long, R. E., Einarsson, P., and Bjornsson, A., 1989, Implosive earthquakes at the active accretionary plate boundary in northern Iceland: Nature, **337**, 640–642.

Foulger, G. R., Miller, A. D., Julian, B. R., and Evans, J. R., 1995, Three-dimensional V_p and V_P/V_s structure of the Hengill triple junction and geothermal area, Iceland, and the repeatability of tomographic inversion: Geophys. Res. Lett., **22**, 1309–1312.

Hamilton, R. M., and Muffler, L. J. P., 1972, Microearthquakes at The Geysers geothermal area, California: J. Geophys. Res., **77**, 2081–2086.

Hearn, B. C., Jr., Donnelly-Nolan, J. M., and Goff, F. E., 1981, The Clear Lake volcanics: Tectonic setting and magma sources, *in* McLaughlin, R. J., and Donnelly-Nolan, J. M., Eds., Research in The Geysers–Clear Lake geothermal area, northern California: U.S. Geol. Surv. Prof. Pap. **1141**, 25–45.

Hudson, J. A., Pearce, R. G., and Rogers, R. M., 1989, Source type plot for inversion of the moment tensor: J. Geophys. Res., **94**, 765–774.

Hulen, J. B. and Nielson, D. L., 1993, Interim report on geology of The Geysers felsite, northwestern California: Trans. Geotherm. Res. Council., **17**, 249–258.

Isherwood, W. F., 1981, Geophysical overview of The Geysers, *in* McLaughlin, R. J., and Donnelly-Nolan, J. M., Eds., Research in The Geysers–Clear Lake geothermal area, northern California: U.S. Geol. Surv. Prof. Pap. **1141**, 83–96.

Iyer, H. M., Oppenheimer, D. H., Hitchcock, T., Roloff, J. N., and Coakley, J. M., 1981, Large *P*-wave delays in The Geysers–Clear Lake geothermal area, *in* McLaughlin, R. J., and Donnelly-Nolan, J. M., Eds., Research in The Geysers–Clear Lake geothermal area, northern California: U.S. Geol. Surv. Prof. Pap. **1141**, 97–116.

Julian, B. R., and Foulger, G. R., 1996, Moment tensors from linear inversion of body-wave amplitude ratios: Powerful constraints on earthquake mechanisms: Bull. Seismol. Soc. Am., **86**, 972–980.

Julian, B. R., and Gubbins, D., 1977, Three-dimensional seismic ray tracing: J. Geophys., **43**, 95–113.

Julian, B. R., Miller, A. D., and Foulger, G. R., 1993, Non-shear Focal Mechanisms of Earthquakes at The Geysers, CA, and Hengill, Iceland, Geothermal Areas: Trans. Geotherm. Res. Council, **17**, 123–128.

———1997a, Non-double-couple earthquake mechanisms at the Hengill-Grensdalur volcanic complex, southwest Iceland: Geophys. Res. Lett., **24**, 743–746.

———1997b, Non-double-couple earthquakes, I Theory: Geophys. Rev., in press.

Julian, B. R., Ross, A., Foulger, G. R., and Evans, J. R., 1996, Three-dimensional image of reservoir depletion at The Geysers geothermal area, California, using V_P/V_S ratio: Geophys. Res. Lett., **23**, 685–688.

Kerr, R. A., 1991, Geothermal tragedy of the commons: Science, **253**, 134–135.

Kirkpatrick, A., Peterson, J. E., and Majer, E. L., 1995, Microearthquake monitoring at the southeast Geysers using a high-resolution digital array: Proc. 20th Workshop on Geotherm. Reservoir Engineering, 79–89.

———1996, Source mechanisms of microearthquakes at the southeast Geysers geothermal field, California: Proc. 21st Workshop on Geotherm. Reservoir Engineering, 359–366.

Kissling, E., Ellsworth, W. L., Eberhart-Phillips, D., and Kradolfer, U., 1994, Initial reference models in local earthquake tomography: J. Geophys. Res., **99**, 19 635–19 646.

Lange, A. L., and Westphal, W. H., 1969, Microearthquakes near The Geysers, Sonoma County, California: J. Geophys. Res., **74**, 4377–4378.

Lofgren, B. E., 1981, Monitoring crustal deformation in The Geysers–Clear Lake region, *in* McLaughlin R. J., and Donnelly-Nolan, J. M., Eds., Research in The Geysers–Clear Lake geothermal area, northern California: U.S. Geol. Surv. Prof. Pap. **1141**, 139–148.

Majer, E. L., and McEvilly, T. V., 1979, Seismological investigations at The Geysers geothermal field: Geophysics, **44**, 246–268.

Miller, A. D., 1996, Seismic structure and earthquake focal mechanisms of the Hengill volcanic complex, S. W. Iceland: Ph.D. thesis, Univ. Durham.

Miller, A. D., Foulger, G. R., and Julian, B. R., 1997, Non-double-couple earthquakes, II Observations: Rev. Geophys., **36**, 551–568.

O'Connell, D. R. H., 1986, Seismic velocity structure and microearthquake source properties at The Geysers, California, geothermal area: Ph.D. thesis, Univ. California.

O'Connell, D. R. H., and Johnson, L. R., 1988, Second-order moment tensors of microquakes at The Geysers geothermal field, California: Bull. Seismol. Soc. Am., **78**, 1674–1692.

Oppenheimer, D. H., 1986, Extensional tectonics at The Geysers geothermal area, California: J. Geophys. Res., **91**, 11 463–11 476.

Romero, A. E., Kirkpatrick, A., Majer, E. L., and Peterson, J. E., 1994, Seismic monitoring at The Geysers geothermal field: Trans. Geotherm. Res. Council, **18**, 331–338.

Ross, A., 1996, The Geysers geothermal area, California: Tomographic images of the depleted steam reservoir and non-double-couple earthquakes: Ph.D. thesis, Univ. Durham.

Ross, A., Foulger, G. R., and Julian, B. R., 1996, Non-double couple earthquake mechanisms at The Geysers geothermal area, California: Geophys. Res. Lett., **23**, 877–880.

Shimizu, H., Matsuwo, N., and Ohmi, S., 1988, A non double-couple seismic source: Tensile-shear crack formation in the Unzen Volcanic Region: Seismol. Res. Lett., **59**, 5.

Stark, M. A., 1992, Microearthquakes—A tool to track injected water in The Geysers reservoir, *in* Stone, C., Ed., Monograph on The Geysers geothermal field: Geotherm. Res. Council Special Rep. **17**, 111–117.

Thompson, R. C., 1992, Structural stratigraphy and intrusive rocks at The Geysers geothermal field, *in* Stone, C., Ed., Monograph on The Geysers geothermal field: Geotherm . Res. Council Special Rep. **17**, 59–63.

Thurber, C. H., 1983, Earthquake locations and three-dimensional crustal structure in the Coyote Lake area, central California: J. Geophys. Res., **88**, 8226–8236.

Truesdale, A. H., Walters, M., Kennedy, M., and Lippmann, M., 1993, An integrated model for the origin of The Geysers geothermal field: Trans. Geotherm. Res. Council, 17, 273–280.

Wessel, P., and Smith, W. H. F., 1991, Free software helps map and display data: EOS, **72**, 441 and 445–446.

Williamson, K. H., 1992, Development of a reservoir model for The Geysers geothermal field, *in* Stone, C., Ed., The Geysers geothermal field: Geotherm. Res. Council Special Rep. **17**, 179–188.

Zucca, J. J., Hutchings, L. J., and Kasameyer, P. W., 1993, Seismic imaging for saturation conditions at The Geysers, California: Trans. Geotherm. Res. Council, **17**, 289–293.